Journal of Computational Physics 229 (2010) 3848–3863

Contents lists available at ScienceDirect

Journal of Computational Physics

journal homepage: www.elsevier.com/locate/jcp

Volume-of-fluid algorithm with different modified dynamic material ordering methods and their comparisons

C.D. Sijoy *, Shashank Chaturvedi

Computational Analysis Division, Bhabha Atomic Research Center, Vizag, Visakhapatnam, India

ARTICLE INFO

Article history:
Received 23 October 2009
Received in revised form 19 January 2010
Accepted 25 January 2010
Available online 2 February 2010

Keywords:
VOF
Multi-material
Material ordering
Onion-skin order
Interface reconstruction
Interface advection
Compressible flow
Volume-of-fluid

ABSTRACT

Volume-of-fluid (VOF) interface reconstruction methods are used to define material interfaces to separate different materials in a mixed cell. These material interfaces are then used to evaluate transport flux at each cell edges in multi-material hydrodynamic calculations. Most of the VOF interface reconstruction methods and volume transport schemes rely on an accurate *material order* unique to each computational cell. Similarly, to achieve overshoot-free volume fractions, a *non-intersecting interface reconstruction* procedure has to be performed with the help of a 'material-order list' determined prior to interface reconstruction. It is, however, the least explored area of VOF technique especially for 'onion-skin' or 'layered' model. Also, important technical details how to prevent intersection among different material interfaces are missing in many literature. Here, we present an efficient VOF interface tracking algorithm along with modified 'material order' methods and different interface reconstruction methods. The relative accuracy of different methods are evaluated for sample problems. Finally, a convergence study with respect to mesh-size is performed.

1. Introduction

Numerical simulation of multi-material hydrodynamic phenomena are of great interest for many researchers which led to many computational methods over the past years including Lagrangian, Eulerian, Arbitrary Lagrangian Eulerian (ALE) and mesh-less (SPH) methods. Pure Lagrangian method fails when material deformations are large enough to give severe distortions to computational mesh. In contrast, the Eulerian methods are capable of handling large material deformations with the aid of proper transport algorithms. However, for multi-material hydrodynamic problems, pure Eulerian method demands mixed equation of state (EOS) evaluation in mixed cells [7]. The continuous rezoning of computational mesh (e.g. ALE type) can overcome the limitations of pure Lagrangian method. This method provides accuracy of Lagrangian and robustness of the Eulerian approaches. The difficulties associated with multi-material problems can be rectified using Eulerian or ALE formulations along with specialized method called *interface reconstruction* or *interface tracking*. The Eulerian and ALE formulations permit the material interfaces to be independent of the computational mesh [6]. Few interface reconstruction formulations are, namely, Level set methods [16,17], Lagrangian particle methods [18], VOF methods [1,2,10] and more recently moment-of-fluid (MoF) methods [19,20]. A detailed review on numerical issues on multi-material problems and different possible VOF approaches can be found in [5,14]. In this paper we describe only the VOF perspective along with 'onion-skin' or 'layered' material ordering methods for multi-material problems.

A detailed description of volume-of-fluid method can be found in many literature [1–4,8] and a review on VOF methods can be found in [6]. Hirt and Nicholas were the first to use the term volume-of-fluid (VOF) in [1]. Later, a one-dimensional

* Corresponding author. Tel.: +91 891 2892156; fax: +91 891 2742460.
E-mail address: cjoy_davis@yahoo.co.in (C.D. Sijoy).

0021-9991/$ - see front matter © 2010 Elsevier Inc. All rights reserved.
doi:10.1016/j.jcp.2010.01.031

method called simple line interface calculation (SLIC), is introduced in [9]. This can be extended to two-dimensional case by directional splitting. The SLIC method is only first order accurate. Youngs [10] introduced a two-dimensional piecewise linear interface construction (PLIC) method. His PLIC–VOF method determines orientation of material interface in an element based on the volume fraction in that element and its surrounding eight elements. This method, in general, is second order accurate. The PLIC reconstruction has been extended to a piecewise parabolic interface construction (PPIC) in [11] which gives a third order accurate result. Rudman in his work [12] introduced FCT–VOF algorithm. He has provided a comparison on different VOF algorithms in the same work [12]. Our present formulation follows the work performed by Gueyffier et al. in [3] and Niem et al. in [13]. The algorithm consists of three parts: interface reconstruction, Lagrangian deformation of material interfaces and finally the Eulerian transport (advection). A 'directional-split' advection procedure is used to extend this method into two-dimensional case. Many open VOF literature describes mathematical formulations only for standard material orientations in a computational cell. Here, we provide a generalized solution procedure for different possible cases of material configuration/orientation in a computational cell. Similarly, many VOF methods presented in literature only treat the case of two materials, where *material order* in a computational cell is not important. Benson in [6,14] has provided a general solution for dynamic material ordering. His method can be applied to situations were more than two materials present in a computational cell. However, important technical details how to avoid intersection among material interfaces are missing. Any intersection of material interface in a cell would induce overshoots in volume fractions and may evaluate incorrect transport flux. In [13] a non-intersecting method for material interface reconstruction is given for three material configuration. This is based on a geometric intersection checks on each material interface. Their method clearly avoids intersection among material interfaces. Unfortunately, their method has no extension to more than three materials as the complexity grows exponentially. Mosso and Clancy [15] has introduced a geometrically derived material ordering using center-of-mass (centroid) of each material. According to them this method works well for any number of materials, except when many material interface exists in a cell width or if a poor resolution is used. We have used these methods for a comparative study with modifications in each.

In this paper we report an efficient VOF algorithm using ALE formulation with a special attention to some specific material orientations which are not described by many other authors. Also, we have improved/modified few dynamic material ordering schemes for 'onion-skin' method, namely for methods given in [5,13,15]. A method how to avoid intersection between different material interfaces is given. A comparative study on different material ordering methods along with different interface reconstruction methods are reported. Finally, a convergence study with respect to mesh-size is performed for each method.

2. Volume-of-fluid (VOF) method

2.1. Structured staggered mesh

A fixed Eulerian grid is used with a virtual Lagrangian step calculations. The effect of Lagrangian step is remapped conservatively onto original Eulerian grid at each time-step [5]. A spatially staggered grid: where volume fractions (f^m, m = material number), density (ρ^m), cell mass etc are cell-centered, whereas the velocity components (u, v) are specified at the mid point of cell edges. See Fig. 1 for details. All calculations are one-dimensional in nature and therefore a 'directional-split' advection algorithm is used to extend it into two-dimensional case. Following Gueyffier et al. [3], the VOF formulation can be split into three major parts: Interface construction, Lagrangian deformation of material interfaces and Eulerian transport step. The interface reconstruction is carried out in a fixed Eulerian grid. If there are more than two materials in a cell, a material order unique to this cell has to be determined. This will be performed with the help of 'material ordering' methods. Last step is Eulerian remap step, where the volume of each material in the overlap region between Lagrangian and Eulerian grids are redistributed onto the original grid. Following sections will describe each of these steps in detail.

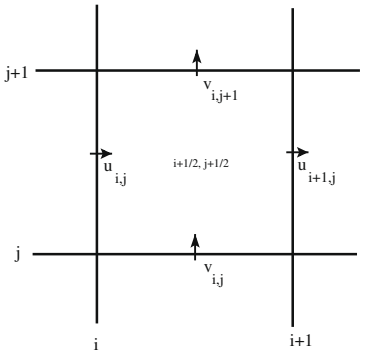

Fig. 1. Schematic of staggered computational grid.

2.2. Interface construction

A piecewise linear interface construction (PLIC) method is used. An interface line can be represented by Eq. (1) [2,10], where $\vec{n} = \hat{i}n_x + \hat{j}n_y$ is the exterior normal to the line and α is the perpendicular distance from a local origin, see Fig. 2 for details. In Fig. 2, only a particular material orientation is shown where both the normal components are positive. Other possible material orientations and corresponding local origins are shown in Fig. 3. It is worth to note that the distance α is always measured from a local origin in our method. It is possible to define α as distance from a common origin. The local origin is defined as per material orientation. For some special cases, e.g. lines parallel to any co-ordinate axis, any one of the possible two origins can be selected.

$$\vec{n} \cdot \vec{x} - \alpha = 0 \tag{1}$$

The slope of a material interface line and hence the normal vector ($\vec{n} = \vec{\nabla} f^m / |\vec{\nabla} f^m|$) can be estimated by using different known existing methods. We have compared four different methods for approximating interface slope. First one is the method given by Parker and Youngs' [10] and the second one is the method given by Gueyffier in [3], which is based on a gradient estimation of average of volume fraction at cell-nodes. The third method is the formulation given in [21] called Youngs' least squares method and the final method is called LVIRA given by Puckett [22]. Details of all these methods can be found in [10,3,21,22]. However, we have provided a short description on these methods in the following sections for a ready reference.

2.2.1. Parker and Youngs' original method [10]

In this 2D method, due to Parker and Youngs [10], the gradient of volume fraction is approximated from a nice cell stencil as described below. This method is considered to be the basis of current generation of two- and three-dimensional VOF methods [6]. However, this method exhibits only first order accuracy [23].

$$\begin{aligned} \nabla_x f_{i,j} &= 0.5(f_E - f_W) \\ \nabla_y f_{i,j} &= 0.5(f_N - f_S) \end{aligned} \tag{2}$$

where,

$$\begin{aligned} f_E &= 0.25(f_{i+1,j-1}, +2f_{i+1,j} + f_{i+1,j+1}) \\ f_W &= 0.25(f_{i-1,j-1}, +2f_{i-1,j} + f_{i-1,j+1}) \\ f_N &= 0.25(f_{i-1,j+1}, +2f_{i,j+1} + f_{i+1,j+1}) \\ f_S &= 0.25(f_{i-1,j-1}, +2f_{i,j-1} + f_{i+1,j-1}) \end{aligned} \tag{3}$$

2.2.2. Gueyffier's node averaged [3]

In this method the volume fractions from a nine-cell stencil are first averaged to cell-nodes. The gradients to this averaged volume fractions in respective directions are taken as an estimate for slope.

$$\begin{aligned} \nabla_x f_{i,j} &= \frac{f_{i+1,j} - f_{i,j} + f_{i+1,j+1} - f_{i,j+1}}{2\Delta x} \\ \nabla_y f_{i,j} &= \frac{f_{i,j+1} - f_{i,j} + f_{i+1,j+1} - f_{i+1,j}}{2\Delta y} \end{aligned} \tag{4}$$

where,

$$f_{i,j} = 0.25(f_{i-1/2,j-1/2} + f_{i+1/2,j-1/2} + f_{i-1/2,j+1/2} + f_{i+1/2,j+1/2}) \tag{5}$$

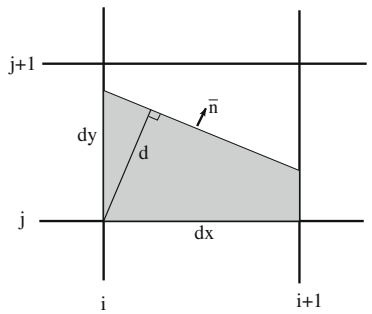

Fig. 2. Geometry of linear interface construction for material interface.

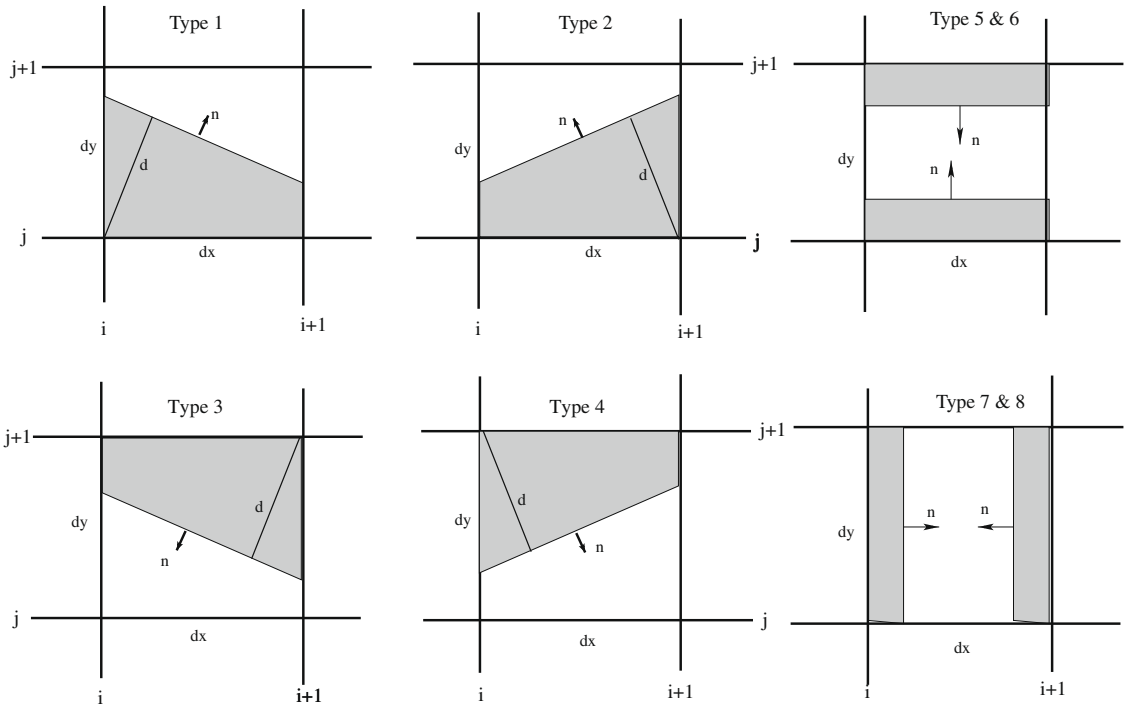

Fig. 3. Different possible material interface orientation.

2.2.3. LVIRA [22]

In LVIRA algorithm one minimizes $E^2_{i,j}$ as a function of slope by rotating the line under the constraint that this line exactly reproduces the volume fraction in the cell. $E^2_{i,j}$ is defined as follows:

$$E^2_{i,j} = \left(\sum_{k,l=-1}^{1} (\tilde{f}_{i+k,j+l}(\tilde{m}) - f_{i+k,j+l})^2 \right)^{\frac{1}{2}} \tag{6}$$

where, $\tilde{f}$ be a linear approximation to a curve passes through the cell (i,j) with slope $\tilde{m}$ and volume fractions $\tilde{f}_{k,l}$. Similarly, $f_{k,l}$ represent the volume fractions due to a true linear function f. The basic logic in the LVIRA algorithm is to minimize some measure of the error between the volume fractions given by the true and approximate interfaces. This method generally exhibits second order accuracy. However, this method seems to be rather costly as a result of least squares problem and implicit estimate of slope [23]. More details can be found in [22,4].

2.2.4. Young's second method [21]

In this method (see [2,21,23] for details), volume fraction Taylor series expansions are formed from each reference cell volume fraction f_i at point $\vec{x}_i$ to each cell neighbor f_k at point $\vec{x}_k$. The square of difference of this quantity to f_k over all n immediate neighbors is then minimized using least squares [2]. This L_2 norm minimization leads to a linear system of equations which can be solved to yield volume fractions gradients and hence normal $\vec{n}$. A simpler approach [23] using Youngs second method by changing the weight factor in Youngs formulation is used here. Their formulation reduces to simple explicit calculation for slope estimate. More details can be found in [23].

2.3. Volume behind interface line

The volume behind an interface line represented by Eq. (1) can be calculated by using methods given in [3,13,6]. However, those formulations are given for standard material orientations where both $n_x,\ n_y > 0$ as in Fig. 2. We have used a method similar to Rider and Kothe [2] for evaluating volume of the material behind interface line. This method explicitly constructs the points of polygon enclosing the fluid in a cell with a known interface line parameters by checking intersection between material interface line and cell boundaries. Different possible orientation for material interface in a computational cell is depicted in Fig. 3. We have developed a generalized algorithm (in order to treat all possible material orientations) for evaluating volume behind material interface line for arbitrary material orientation with a given interface line parameters, (see Appendix A for an outline of the algorithm).

2.4. Volume iteration

Having obtained interface normals the interface parameter α has to be determined (see Eq. (1)) so that volume behind the interface line is equal to the material volume. If there are more than two materials in a cell a material order has to be determined and all materials are layered in that order so that volume behind ith and $i-1$th material interface is equal to the sum of volume of materials from 1 to $i-1$. Different methods for evaluating 'material order' will be discussed in later sections. The interface parameter α is found when the function $f(\alpha) = V(\alpha) - V_{actual}$, becomes zero. Here, $V(\alpha)$ is the material volume in the cell bounded by the interface line with line parameter α. An efficient *root-finding* algorithm can be used to find α. We have used *Brents* method for root-finding as suggested in [2]. In our calculation we have used $\alpha_{\min} = 0$ and $\alpha_{\max} = d$ as initial bracket for root-finding system, where 'd' is the cell diagonal distance. For each iteration in root-finding system a function which evaluate volume behind an interface line with a given interface parameters has to be used. We have used our new volume evaluation algorithm mentioned in Section 2.3.

2.5. Multi-material interface construction

In this section we describe a 'non-intersecting' material interface construction method. Once the 'material order' is defined (how to define material order is discussed in later sections), the material interfaces are constructed using methods given in Section 2.2 using 'onion-skin' model. Given a material order, material m_1 to m_N, the first interface, between m_1 and m_2, is calculated by putting the volume of m_1 behind the interface [6]. The slope of this particular material is evaluated by using the volume fractions of material m_1 in a 3×3 block element surrounding it (see Fig. 4).

The second interface, between m_2 and m_3, is calculated by putting the volumes of m_1 and m_2 behind the interface. This time the sum of volume fractions between m_1 and m_2 in 3×3 block is used for evaluating slope. In general, the interface of material i is constructed by putting the sum of the volumes of materials m_1 through m_i behind interface i and same logic is applied for slope estimate. There is no guarantee that a pair of interfaces within a mixed cell will not intersect by this method [6]. Such cases are not addressed in open literature. Any intersection of material interface in an element will give rise to overshoot in volume fractions and may lead to incorrect mass transport for material density. We have rectified this difficulty by using our method (motivated from [13]) which is described below. Once the interface reconstruction is completed, we check for an intersection among them in order. If there is an intersection, the scalar product of their normal vector $(\vec{n}_{m1} \cdot \vec{n}_{m2})$ is evaluated [13]. If the scalar product is negative, we determine a new interface for material having lesser volume fraction among them by using Eq. (7) (In Eq. (7) we have assumed $f^{m_1} > f^{m_2}$).

$$\vec{n}_{m_2} = \frac{\vec{n}_{m_2}}{|\vec{n}_{m_1}|} - \frac{\vec{n}_{m_1}}{|\vec{n}_{m_2}|} \tag{7}$$

If the scalar product is positive, we adjust the normal of least stiff material equal to the normal of other material. Thereafter, new interface parameter, α is evaluated. This method may introduce a slight deviation to the normals estimated earlier. However, errors due to intersection among material interfaces are removed, which are more important than a slight error in material orientation. Remember, the normal estimation by using any standard methods given in Section 2.2 are again an approximation, which can be either first order or second order accurate. Therefore, a slight modification just enough to avoid intersection can be justified.

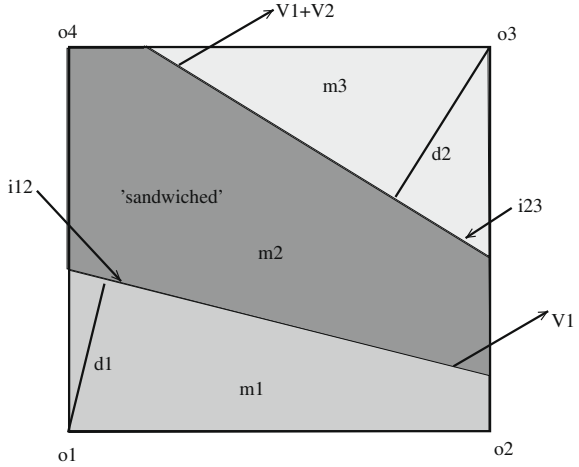

Fig. 4. Onion-skin order of material interfaces in a computational cell.

2.6. Dynamic material ordering

When a multi-material cell contains more than two materials, a material interface has to be determined for each pair of materials. A typical three material configuration is depicted in Fig. 4. These material interfaces are constructed using 'onion-skin' or 'layered' model. In this study, we will describe only 'onion-skin' model, where materials are layered in a specific order with non-intersecting interfaces. Therefore, present scheme cannot accurately model *triple point*, *Y-junction* and *T-junction* within a cell. Modeling of *triple point*, *Y-junction* and *T-junction* within a cell can be achieved using methods given in [19,20] (MoF), [25] (PLIC). However, these methods then require more complicated volume advection schemes. Recent work in [24] used MoF method with material compressibility. Our aim is to provide a relatively simple advection and material ordering methods for practical multi-material problems. Situations with triple points, *T*-junction etc. can be resolved with reasonable accuracy by using highly refined mesh. The 'onion-skin' order method for determining material order has been used successfully for many multi-material compressible hydrodynamic problems [5,13] including micro-mechanics [14]. Detailed discussions on different material ordering methods are given in following sections. We have modified/improved few existing methods and introduced a simple material ordering method by using a combination of two different approaches.

2.6.1. Niem's intersection check method

In this section we discuss on a method given in [13]. This method is based on an intersection check between material interface lines. This method works only for three material configuration in a mixed cell. First, an independent interface reconstruction for each material is performed. Second step is to test for an intersection point of each pair of interface lines within a cell. This can be performed by a simple line intersection check with known interface line parameter α and their slopes. The final goal is to eliminate one out of three interface lines to partition the cell into an 'onion-skin'. Counting each intersection among a particular pair of interface lines independently, there are $2^3 = 8$ different cases [13]. These are listed in Table 1. Third step is to reject the interface line of one of the materials. The rejected material is then 'sandwiched' in between the two others. We have used this particular method to choose two materials polygons having non-intersecting interface. Thereafter, a 'material order' for *volume transport* is assigned by identifying their local origin. We discuss these modifications in details here. First, we introduce a 'joint parameter' $j_m(i) = 1$, if two material polygon have an overlapping area. This parameter will be used later for volume transport. The material ordering is performed as follows. Firstly, if the material polygons (not for sandwiched material) are disjoint ($j_m(i) = 0$), we search for a material polygon which contains both of the lower corners. If there is no such case, search for a material polygon which contains left bottom corner of the cell. If none of the material polygons contains left bottom corner, same procedure will be repeated for right bottom corner (anti-clockwise). The first member in the material order list is one having both of the lower corners. If none of the material is having those corners, numbering is done as per the corner occurrence in material polygon in anti-clockwise direction. Secondly, if the material polygons are joint ($j_m(i) = 1$), we identify their common local origin and sum of material volume in cells around their local origin is calculated. Finally, a material order is assigned as per material abundance in those cells. The solutions provided in [13] for all the cases listed in Table 1, will not be discussed here. Details of these cases can be found in [13]. For each of these cases, first we choose two disjoint polygons using methods in [13] and finally we perform our geometrical test for assigning material order along with 'joint parameter' which is later used for volume transport. Additional modification is required if a mixed cell contains background material. In such cases we prefer to put background material always second in the list [14].

2.6.2. Centroid check method by Mosso and Clancy

Mosso and Clancy [15] developed a formulation based on approximate center-of-mass of materials. They evaluate the centroid (x_m) from a nine-cell stencil centered by the mixed cell from the material volume fractions and cell centroids (x_c) as given Eq. (8).

$$x_m = \frac{\sum_{i=1}^{9} f^m(i) x_c(i)}{\sum_{i=1}^{9} f^m(i)}, \quad m = 1, \ldots, M \tag{8}$$

Once all the centroids are evaluated, the materials are arranged in the ascending order of their centroid distances from a 'local origin'. This 'local origin' is determined by checking slope of lines connecting material centroids. A positive slope is

Table 1
Different cases of intersection among pairs of interface lines [13]; 'y' and 'n' stands for an intersection and non-intersection, respectively.

Case	Lines 1 and 3	Lines 2 and 3	Lines 1 and 2	Decision
1	n	n	n	Reject 1, 2 or 3
2	n	n	y	Reject 1 or 2
3	n	y	n	Reject 2 or 3
4	y	n	n	Reject 1 or 3
5	n	y	y	Reject 2
6	y	n	y	Reject 1
7	y	y	n	Reject 3
8	y	y	y	Adjust normal

a vote for the lower left corner and a negative slope is a vote for the lower right corner [6], see Fig. 5. If the background material is first in the material order list, we modify the material order in such a way that the background material will be always second in the list as per suggestions given in [14]. This dynamic material ordering work well for any number of materials except when many interfaces exists within a cell width. Again, there is no guarantee that a pair of interfaces within a mixed cell will not intersect. Therefore, once the 'material order' is defined, the interface reconstruction in multi-material cell follows our method given in Section 2.5. The 'joint parameter', $j_m(i)$ is set equal to one for all materials except for the first material in the 'material order' list.

2.6.3. A simple combination of Centroid check and Benson's least squares fit to centroid

A similar approach is described by Benson in [14]. He adds the locations of the centroids as solution variables. They are transported using some higher-order transport algorithm, e.g. MUSCL algorithm [14]. Using the centroids of the materials $(\vec{x}_m)$ in the current element, a least squares fit to a line is calculated by solving the least squares problem given in Eq. (9).

$$\min\ J = \frac{1}{2}\sum_{m=1,M} f^m[n_x(x_m - \tilde{x}) + n_y(y_m - \tilde{y})]^2 \tag{9}$$

The projections of the centroid locations onto this line are sorted in ascending order. There after few *heuristic rules* are applied to define 'material order', details of these rules and their purpose can be found in [14]. See Fig. 6. This method is found to be more accurate in determining 'material order'. We actually did not transport material centroids, instead an approximate centroid for each material is evaluated at each time-step using method given by Mosso and Clancy [15]. Remaining procedures follows method given by Benson in [14]. Here, 'joint parameter', $j_m(i)$ is set equal to one for all materials except for the first material in the 'material order' list. Finally, to avoid intersection among material interfaces within a cell, we use our method given in Section 2.5.

2.7. Calculation of advected or transported volume

The volume fraction, f^m for each material is updated at each time-step by solving an advection equation (color advection) of the form given by Eq. (10), see [1,2,13,23].

$$\frac{\partial f^m}{\partial t} + u\frac{\partial f^m}{\partial x} + v\frac{\partial f^m}{\partial y} = 0 \tag{10}$$

The advected volume, $V_i^{m,a}$ for each material m through a cell face i is evaluated in 'flux difference' form as suggested in [13] along with volume evaluation algorithm mentioned in Appendix A. This particular method is a perfectly overshoot-free and economic algorithm. Detailed mathematical formulation can be found in [13]. Here, we describe only the modifications performed in our algorithm to treat different possible material orientations. The Lagrangian deformation changes the interface normal and line constant, α in such a way that so-called the wetted area is invariant [13,3]. Therefore, the effect of material interface during x-direction sweep can be written as,

$$\begin{aligned} \tilde{n}_x &= \frac{n_x \Delta x}{\Delta x + (u_{i+1} - u_i)\Delta t} \\ \tilde{n}_y &= n_y \\ \tilde{\alpha} &= \alpha + \tilde{n}_x u_i \Delta t \end{aligned} \tag{11}$$

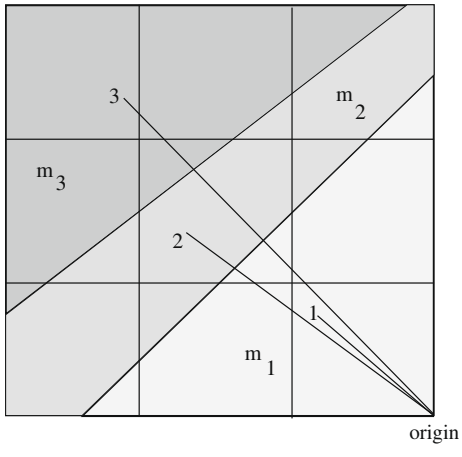

Fig. 5. Priority checking by Mosso–Clancy method.

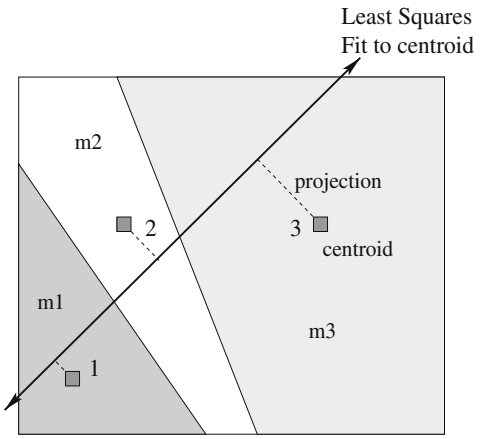

Fig. 6. Priority checking by Benson's method of least square fit to the set of the centroids.

refer [3,13] for its general mathematical formulations. The calculation of advected volume is now equal to the evaluation of the area of the overlap region between Eulerian and Lagrangian positions after deformation (see Fig. 7), which is calculated using new interface parameters after Lagrangian deformation. Our method for evaluating advected volume for all possible material orientations during x-direction sweep is described below. First, we determine the donor cell at each cell face by checking velocity sign. It is worth to note that all advected volumes have the same sign as the velocity at that face. If the interface slope, n_x is positive (see Fig. 7) for a particular material (m) in the donor cell; the volume advected for this material right to donor cell is evaluated by using new interface parameters [13] given below as arguments to algorithm given in Appendix A.

$$\begin{aligned} \tilde{\alpha} &= \alpha - n_x \Delta x + \tilde{n}_x u_{i+1} \Delta t \\ \Delta \tilde{x} &= u_{i+1} \Delta t \end{aligned} \tag{12}$$

The advected volume calculated in this way is the sum of transport volumes of the group of the materials behind this particular interface. Therefore, if the 'joint parameter', $j_m(i)$, defined while material ordering is equal to one; then the advected volume for this particular material (m) is obtained by calculating difference of $V_i^{m,a}$ and $V_i^{m-1,a}$. If the slope of interface, n_x is negative (see Fig. 8) for a particular material (m) in the donor cell; the volume advected is calculated with $\tilde{\alpha} = \alpha$ (remaining parameters are same as given in Eq. (12)), see [13] for a mathematical proof. Similarly, the volume advected to a cell left to the donor cell (if $u_i < 0$) is evaluated as follows. If the interface slope in the donor cell, n_x is negative; the volume advected left to donor cell is evaluated by using new line interface parameters given below.

$$\begin{aligned} \tilde{\alpha} &= \alpha + n_x \Delta x + \tilde{n}_x u_i \Delta t \\ \Delta \tilde{x} &= |u_i \Delta t| \end{aligned} \tag{13}$$

If the slope, n_x is positive; the advected volume in the acceptor cell is calculated using $\tilde{\alpha} = \alpha$ and $\Delta \tilde{x} = |u_i \Delta t|$. In all these cases new normal $(\tilde{n}_x)$ is evaluated as in Eq. (11) and $\Delta \tilde{y} = \Delta y$. Special cases, when any of the normal component vanishes (when interfaces are parallel to co-ordinate axis), are treated separately, see Fig. 9. If the normal components are $(n_x, n_y) = (1, 0)$

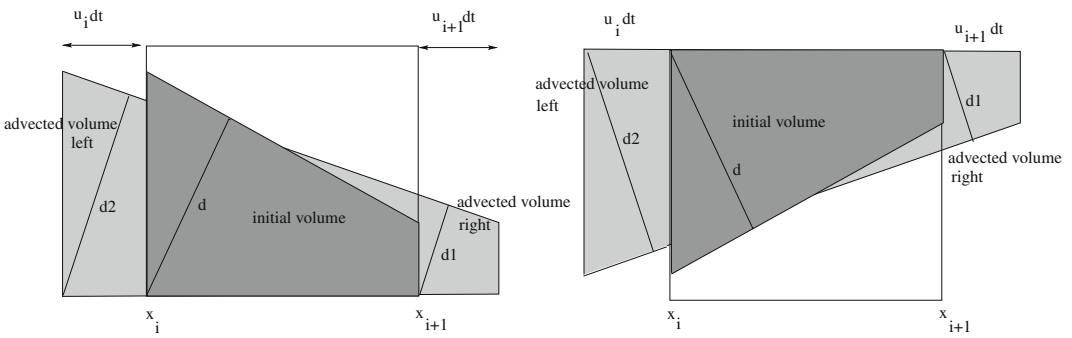

Fig. 7. Material polygon before and after Lagrangian deformation for two different orientations.

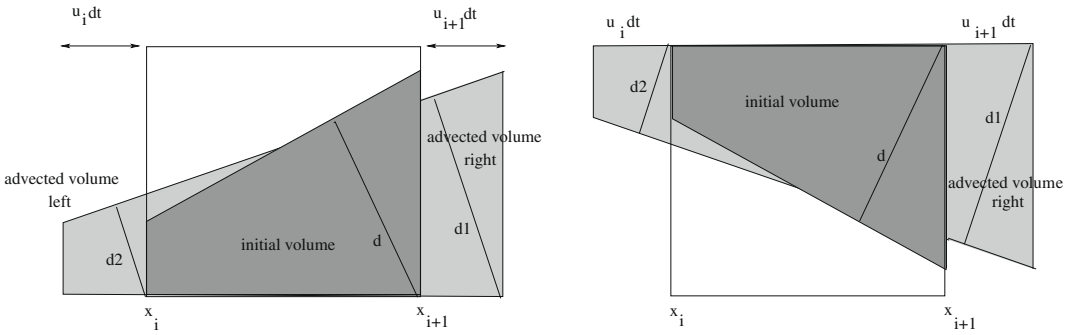

Fig. 8. Material polygon before and after Lagrangian deformation.

then following procedure is followed. Assuming the material interface, x_c moves with linearly interpolated velocity between cell edge velocities, the interface location can be updated by using Eq. (14) given below.

$$\tilde{x}_c = x_c + u_i \Delta t + \frac{x_c - x_i}{\Delta x}(u_{i+1} - u_i)\Delta t \tag{14}$$

The volume advected to a cell right to the donor cell (if $u_{i+1} > 0$) is found if $\tilde{x}_c > x_{i+1}$ with $\tilde{\alpha} = x_{i+1} - x_c, \tilde{n}_x = 1$ and $\tilde{\Delta x} = x_{i+1} - x_c$ as arguments to volume evaluation function. If $\tilde{x}_c \leqslant x_{i+1}$ the advected volume is equal to zero. If $u_i < 0$, the volume advected to a cell left to the donor cell is evaluated using $\tilde{\alpha} = \min(\tilde{x}_c - (x_i + u_i\Delta t), u_i\Delta t)$, $\tilde{n}_x = 1$ and $\tilde{\Delta x} = |u_i \Delta t|$ as arguments. Similar procedure is followed for the case with normal components $(n_x, n_y) = (-1, 0)$. Finally, a flux difference form given in Eq. (15) is used for volume fraction update, which includes the effect of Lagrangian and Eulerian steps in a single expression, see [13] for details.

$$\begin{aligned} f_{i+1/2,j}^{m,n+1} &= f_{i+1/2,j}^{m,n} + \frac{\Delta t}{\Delta x}\left[A_i^m - B_{i+1}^m\right] \\ A_i^m &= \frac{V_i^{m,a}}{\Delta y \Delta t} - u_i f_{i+1/2,j}^m \\ B_i^m &= \frac{V_i^{m,a}}{\Delta y \Delta t} - u_i f_{i-1/2,j}^m \end{aligned} \tag{15}$$

The advection procedure in y-direction (y-sweep) of the directionally-split algorithm follows the same.

3. Results and discussions

The VOF algorithm is tested with different test problems which involves the tearing and stretching of material. The results are compared with known values and an error estimate is performed. We have used an L_1 error norm defined as in Eq. (16).

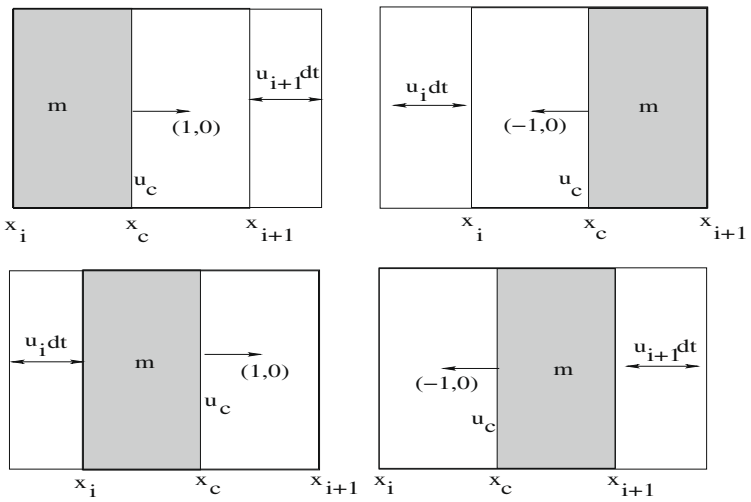

Fig. 9. Material polygon when interfaces parallel to co-ordinate axis. Here x_c and u_c are interface location and velocity, respectively.

$$L_1 = \sum_{i=1,N} \left| f_i^c - f_i^e \right| \times V_i \tag{16}$$

Here, N is the total number of cells in the domain, V_i is the volume of the cell and $f_i^{c,e}$ are the computed and exact volume fractions, respectively. Different interface reconstruction methods, namely, node averaged method [3], Parker and Youngs' method [10], Youngs' second method [23] and LVIRA method are named conveniently as NA, PY, YS and LV, respectively. Similarly, material ordering methods are named MC (Mosso and Clancy), NI (Niem's intersection check method) and MB (combination of MC and Benson's least squares method). For all calculations presented here, we have used Courant number equal to 0.5 for time-step calculation.

3.1. Vortex test: two materials

The VOF algorithm is tested with two material configuration where the second material is the background material [2]. The computational domain is a unit square with a circle of radius 0.15, centered at (0.5,0.75). The velocity fields are given by Eq. (17).

$$\begin{aligned} \Psi &= \frac{1}{\pi} \sin^2(\pi x) \sin^2(\pi y) \cos(\pi t/T) \\ u &= -\frac{\partial \Psi}{\partial y}, \quad v = \frac{\partial \Psi}{\partial x} \end{aligned} \tag{17}$$

Note that the vortex velocity fields are multiplied by a factor $\cos(\pi t/T)$, giving a flow that returns to its initial state at $t = T$ and at $t = T/2$ the material undergoes maximum distortion. The reversal period used here is $T = 8.0$, which produce a maximal stretch at $t = 4.0$. Fig. 10 shows the result of the vortex test with combination NA + NI and with 64×64 mesh at two different times ($t = T/2$ and $t = T$). In Table 2, the error norms for different methods discussed in earlier sections are tabulated for different grid resolutions. Convergence test results for this case shows that the overall algorithm for all cases shows nearly second order convergence, similar to one reported in [2]. The solution error decreases considerably as grid is refined. The combination of LVIRA and Niem's intersection check method gives better accuracy for this case. However, as grid resolution increases this combination gives almost same accuracy to other methods.

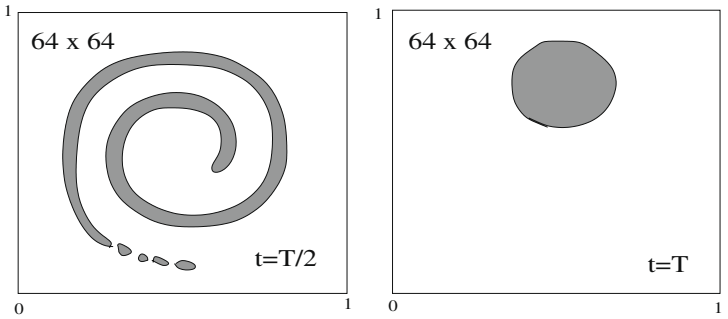

Fig. 10. Result of reversed single vortex with 64×64 mesh at $t = T/2$ and $t = T$; where, $T = 8.0$.

Table 2
Comparison of the L_1 norm errors for the single vortex test with two materials.

Method	32×32	64×64	128×128
NA + NI	3.799e−2	6.669e−3	1.369e−3
NA + MC	3.859e−2	6.685e−3	1.370e−3
NA + MB	3.819e−2	6.699e−3	1.374e−3
PY + NI	3.819e−2	6.629e−3	1.368e−3
PY + MC	3.899e−2	6.658e−3	1.372e−3
PY + MB	3.869e−2	6.669e−3	1.378e−3
YS + NI	3.749e−2	6.569e−3	1.366e−3
YS + MC	3.819e−2	6.574e−3	1.367e−3
YS + MB	3.789e−2	6.583e−3	1.368e−3
LV + NI	3.719e−2	6.559e−3	1.364e−3
LV + MC	3.769e−2	6.576e−3	1.365e−3
LV + MB	3.759e−2	6.591e−3	1.364e−3

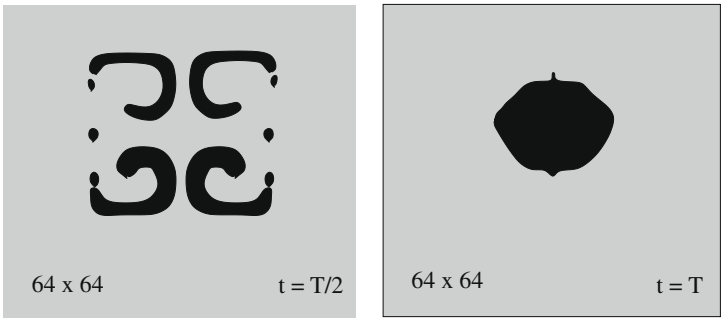

Fig. 11. Result of reversed deformation test with 64×64 mesh at $t = T/2$ and $t = T$; where, $T = 2.0$.

It is clear form Table 2 that the LVIRA method performs better compared to other methods (NA, PY and YS) for slope calculation. Therefore, in the following sections we consider only LVIRA method along with different dynamic material ordering methods (MC, NI and MB).

3.2. Deformation velocity field test: two materials

In this case a deformation velocity field represented by Eq. (18) (introduced in [2]) is used. This leads to a test more difficult than vortex test with extreme deformations. Ideally, the solution goes back to original state at $t = T$ due to the multiplication factor $\cos(2\pi t/T)$ with period T. The initial position of the circle was $(0.5, 0.55)$, and a period $T = 2.0$ is used. The solution by using LV + NI method for $t = T/2$ and $t = T$ with a 64×64 mesh is shown in Fig. 11. Since, the numerical solution returns to initial state, L_1 norm error estimate can be used. Table 3 lists the L_1 norm error with different combination of methods. In this case, when a low-resolution is used the LV + MB method gives better accuracy. The Benson's least squares method found to be superior when an irregular deformation occurs (without much tearing and fragmentation of the materials), even-though the variation from other results are less.

$$\begin{aligned} \Psi &= \frac{1}{4\pi}\sin(4\pi x + 2\pi)\cos(4\pi y + 2\pi)\cos(2\pi t/T) \\ u &= -\frac{\partial \Psi}{\partial y}, \quad v = \frac{\partial \Psi}{\partial x} \end{aligned} \tag{18}$$

Further, to differentiate the results between different methods, the L_1 norm errors are compared at later times ($T = 6.0$). The results are summarized in Table 4. The increased period (more deformation) produces tearing and fragmentation of the materials. Benson's method produces better accuracy when material tearing and fragmentation occurs. The error with Niem's intersection method is higher (for coarser mesh) due to the fact that this method rely on accurate slope estimate and intersection checks based on it. Remember, that the slopes are estimated using volume fractions from the neighboring cells. Large deformations with material tearing and fragmentation leads to many empty cells around a material filled cell. This further leads to incorrect slope estimate and hence the material ordering with NI method. However, the L_1 norm error and the error difference between different methods are found to be decreased with finer meshing. It is also observed that final material state obtained after one complete period using NI and MC methods contains void volumes which are absent

Table 3
Comparison of the L_1 norm errors for deformation test with two materials at $t = 2.0$.

Method	32×32	64×64	128×128
LV + NI	1.998e−2	1.151e−2	5.967e−3
LV + MC	1.989e−2	1.144e−2	5.965e−3
LV + MB	1.974e−2	1.132e−2	5.964e−3

Table 4
Comparison of the L_1 norm errors for deformation test with two materials at $t = 4.0$.

Method	64×64	128×128
LV + NI	2.169e−1	2.706e−2
LV + MC	1.529e−1	2.452e−2
LV + MB	1.065e−1	2.214e−2

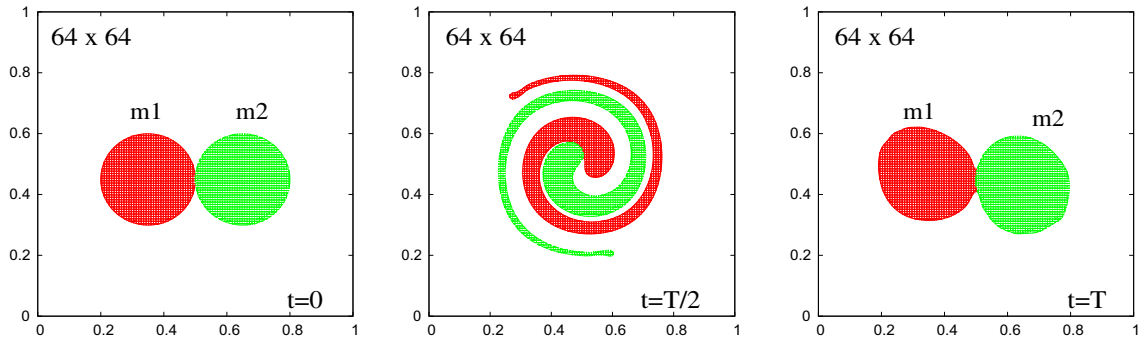

Fig. 12. Reversed vortex test for two circles with 64×64 mesh at $t = T/2$ and $t = T$; where, $T = 8.0$.

in the initial state. This situation is also reported in [13] for NI method. The accuracy of MC method is in between that of MB and NI methods.

3.3. Vortex test: three materials

In this test we choose two different material blots in a background material. The radius of each blots were 0.15 and located at (0.35,0.45) and (0.65,0.45), respectively. The velocity field represented by Eq. (17) is used with period $T = 8.0$. Fig. 12 shows the configuration of materials at $t = 0,\ t = T/2$ and $t = T$ by using method LV + MB. The calculated L_1 norm error for various cases shows similar trend as given in Table 2; even-though they slightly differ in magnitude we have not listed those values here for brevity. However, with increased period $T = 16.0$ on a coarser mesh, the errors with different methods are easily differentiable. The calculated L_1 norm errors, with a mesh resolution of (32×32), are given in Table 5. As earlier, the MB method gives better accuracy on coarser mesh. The difference in errors between MB and MC methods are less due to the fact that both methods are based on material centroid locations.

3.4. Deformation velocity field test: three materials

Next, we have applied a deformation field velocity for three material configuration, where two blots of different material are kept on a third material (background material). The velocity field is given in Eq. (18) with period $T = 2.0$ and $T = 4.0$. The computed solution for material configuration is shown in Fig. 13. The L_1 norm error calculated for this case with $T = 2.0$ shows the trend as listed in Table 3, which we have not listed here for brevity. However, with period $T = 4.0$ and a mesh

Table 5
Comparison of the L_1 norm errors for the single vortex test $(T = 16.0)$ with three materials.

Method	32×32
LV + NI	5.732e−2
LV + MC	4.998e−2
LV + MB	4.855e−2

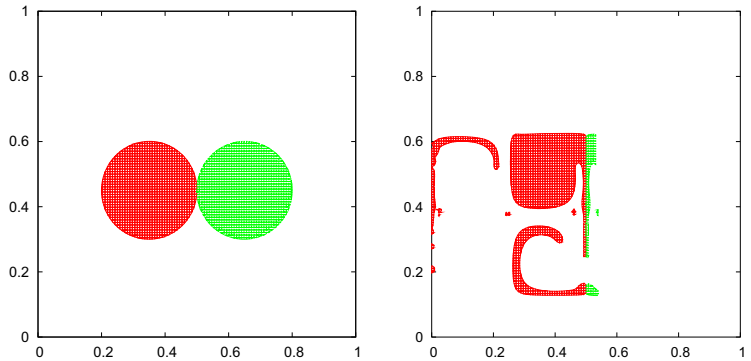

Table 6
Comparison of the L_1 norm errors for deformation velocity field test ($T = 4.0$) with three materials.

Method	32×32
LV + NI	6.231e−2
LV + MC	5.285e−2
LV + MB	5.006e−2

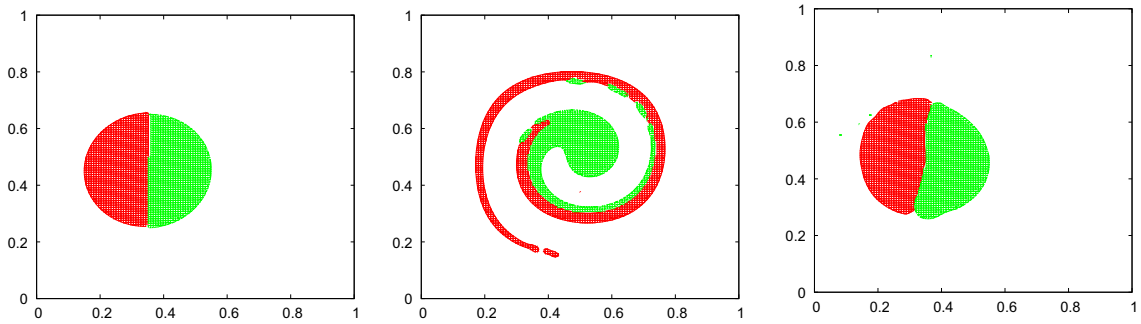

Fig. 14. Reversed vortex test for a single blot consists of two different materials with 64×64 mesh at $t = T/2$ and $t = T$; where, $T = 8.0$.

resolution of (32×32), the difference in errors with different methods are noticeable. Table 6 summarizes the L_1 norm errors for this case. For irregular material deformation the difference in errors between NI and MC/MB method is found to be higher than that of vortex test on coarser grids. Also, material fragment mixing is observed in all cases.

3.5. Vortex test: three materials with triple point

In this numerical experiment we choose a single blot consists of two different materials (half circles) in the background material. This particular geometry consists of two triple points in the computational domain. These triple points introduce additional complexity to the material ordering methods. The velocity field represented by Eq. (17) is used with period $T = 8.0$. The radius of this blot was 0.2 and located at (0.35,0.45). Fig. 14 shows the configuration of materials at $t = 0,\ t = T/2$ and $t = T$ by using method LV + MB. The calculated L_1 norm error for various methods are given in Table 7.

Table 7
Comparison of the L_1 norm errors for reversed vortex test for a single blot consists of two different materials at $t = 8.0$.

Method	32×32	64×64	128×128
LV + NI	3.205e−2	1.436e−2	6.163e−3
LV + MC	2.906e−2	1.285e−2	6.015e−3
LV + MB	2.283e−2	1.106e−2	5.954e−3

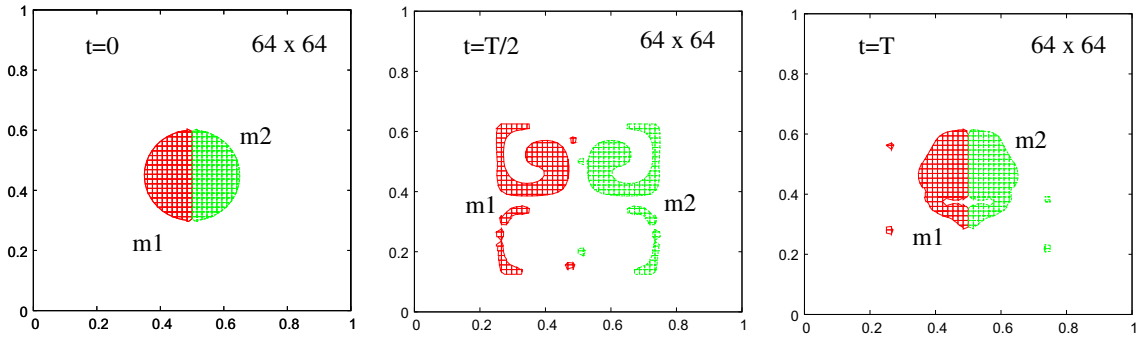

Fig. 15. Result of reversed deformation test with 64×64 mesh at $t = T/2$ and $t = T$; where, $T = 2.0$.

Table 8
Comparison of the L_1 norm errors for deformation test with three materials at $t = 2.0$.

Method	32×32	64×64	128×128
LV + NI	3.048e−2	1.606e−2	6.125e−3
LV + MC	2.374e−2	1.367e−2	6.098e−3
LV + MB	2.104e−2	1.246e−2	5.998e−3

The final state obtained with LVIRA + MB method shows better overlap with initial state. All the three methods tend to over-smooth the interface. The reason for this is that all PLIC–VOF methods, due to their dependency to spacial volume fraction profiles while estimating interface normals, have a tendency to smooth-out the interface. However, with decreased mesh-size (fine meshing), this smoothing effect can be globally minimized. As before, with a coarser mesh MB method produces better accuracy.

3.6. Deformation velocity field test: three materials with triple point

In this case a deformation velocity field represented by Eq. (18) is used. This leads to a test more difficult than vortex test with extreme deformations for material triple point. The initial position of the circle was $(0.5, 0.45)$, and a period $T = 2.0$ is used. The solution by using LV + MB method for $t = T/2$ and $t = T$ with a 64×64 mesh is shown in Fig. 15. Table 8 lists the L_1 norm error with different methods. In this case, when a low-resolution is used the LV + MB method gives better accuracy. The Benson's Least squares method found to be superior when an irregular deformation occurs. It is clear from Fig. 15 that the final state obtained contains background material (material-3) when coarser mesh is used. Also, material fragments are observed around the blot in all cases with coarser mesh.

3.7. Shock tube problem: three materials with triple point

Further, we demonstrate the performance of ALE–VOF algorithm with different material ordering methods for a shock tube problem [26]. This involves the hydrodynamic evolution of a material triple point. The initial material configuration is depicted in Fig. 16 and the initial material state values used are summarized in Table 9. Ideal gas equation state is used for hydrodynamic pressure evaluation for each material. A volume weighted pressure calculation is used for calculating total pressure in mixed cells. This material configuration consists of a triple point (T-junction). The high pressure material (left side) creates a shock wave which propagates along positive x-direction. Due to different material properties this shock wave travels faster in one material leading to a vortex evolution around the triple point.

The results are compared against the computational results obtained by using a finer mesh (560×240) due to the lack of analytical solution to this problem. With increased resolution $(140 \times 60,\ 280 \times 120$ etc.), the three methods exhibits almost same accuracy level. On a coarser mesh 80×40 the MC and MB method shows better accuracy during initial stage. However,

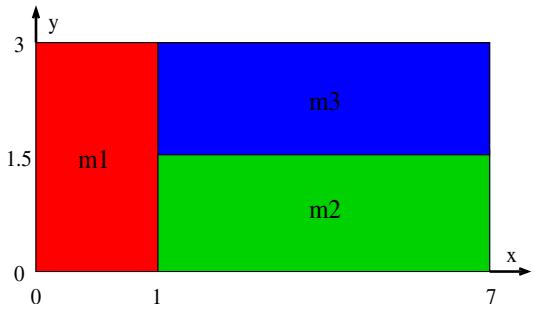

Fig. 16. Initial conditions for triple point shock tube problem. The materials are at rest at $t = 0$.

Table 9
Initial material state values for three material shock tube problem.

Quantity	Material-1 (m1)	Material-2 (m2)	Material-3 (m3)
Density (ρ)	1.0	0.1	0.125
Gamma (γ)	1.5	1.4	1.5
Pressure, p	1.0	0.1	0.1
Initial velocity, u	0.0	0.0	0.0

Table 10
Comparison of the L_1 norm errors for shock tube problem with three materials at $t = 2.4$ s.

Method	80×40	140×60	280×120
LV + NI	1.04e−1	1.36e−3	2.72e−4
LV + MC	0.87e−1	1.23e−3	2.64e−4
LV + MB	0.70e−1	1.20e−3	2.59e−4

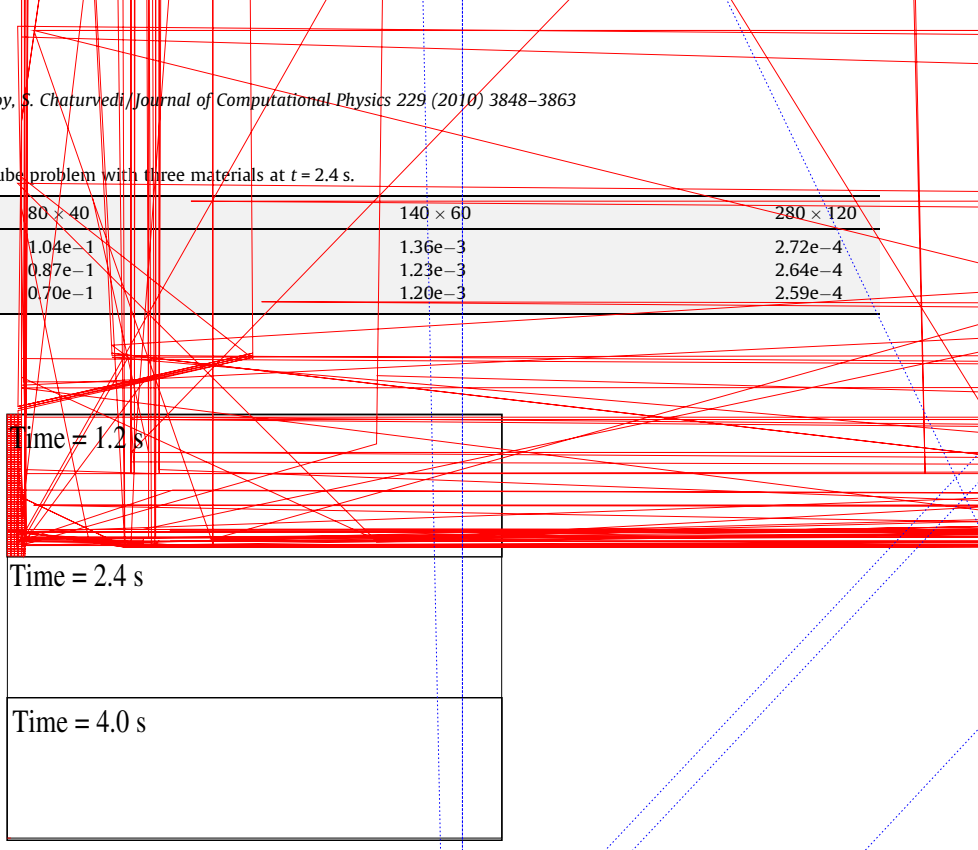

Fig. 17. Evolution of material triple point for three material shock tube problem with 140×60 mesh resolution. The plots are shown at $t = 1.2$, 2.4 and 4.0 s, respectively.

on later times, all methods suffers material break-up and fragmentation (due to coarser-meshing). In all the cases, once the fragmentation is started the results tends to deviate from expected results. Table 10 lists the L_1 norm error with different methods (see Fig. 17).

4. Summary of comparative study

Among the four methods compared for slope estimate, the LVIRA method is found to be superior. The accuracy of explicitly differenced Young's second method is higher than that of node averaged method (NA) and first order Parker and Youngs (PY) method. The three dynamic material ordering methods, namely, Niem's intersection check method (NI), Mosso and Clancy method (MC) and Benson's method (MB) produce almost same accuracy with finer meshing. Benson's method has an advantage when a coarser-meshing is used for problems involving irregular material deformation. If the mesh resolution used is poor for problems involving large deformations, Niem's intersection method based on interface slope rather than material centroid suffers more. However, the Niem's intersection check method clearly avoids material intersection in multi-material cell without additional effort. Both MC and MB method need to undergo an intersection check once the material ordering and interface reconstruction is completed. The major limitation of NI method is that this method is presently being limited to only three materials, whereas the MB and MC method can be applied to any number of materials in a mixed cell. For complex problems invloving the evolution of material triple point on a coarser grid, the PLIC–VOF algorithm tend to smooth-out the *T*-junction irrespective to the ordering method used. However, with increased spacial resolution triple point evolution can be reasonably resolved.

5. Conclusions

A volume-of-fluid (VOF) algorithm using ALE formulation is provided for compressible multi-material problems with special attention to different possible material orientations. Different interface construction methods are discussed. A method to avoid intersection among material interface lines in a mixed cell is provided. A generalized *algorithm outline* for calculating material volume behind an interface line in a mixed cell is given. Different existing 'material order' methods are discussed and a simple method with the combination of two different methods is introduced. Few numerical test problems are provided to estimate the error and a convergence study with respect to mesh-size is performed. The numerical experiments show that the given algorithm is reasonably accurate for interface reconstruction with different material ordering methods.

Acknowledgments

The authors are thankful to Dr. D.J. Benson (University California, San Diego) [5,6,14], for providing us his manuscripts which helped us in understanding various aspects of material ordering methods. Also, We thank our referees for their valuable comments and helpful suggestions in completing this work.

Appendix A. Algorithm outline for volume behind an interface line

1. Adjust normal depending on orientation

$$\begin{aligned} &if(n_x < 0); \quad \alpha = \alpha + n_x \Delta x \\ &if(n_y < 0); \quad \alpha = \alpha + n_y \Delta y \end{aligned} \tag{A.1}$$

2. Get the two intersection points with cell edges
3. Collect all cell-nodes lies behind an interface line

$$if n_x(x - x_i) + n_y(y - y_i) \leqslant \alpha \tag{A.2}$$

4. Construct a polygon using nodes from steps 2 and 3
5. Calculate volume of this polygon

$$V_{xy} = \frac{1}{2} \sum_{i=1,n} (x_i y_{i+1} - x_{i+1} y_i) \tag{A.3}$$

where n_x is the normal component along x-direction; n_y is the normal component along y-direction; α is the perpendicular distance to interface line from local origin; Δx is the mesh-size along x-direction; Δy is the mesh-size along y-direction; n is no. of polygon nodes.

References

[1] C.W. Hirt, B.D. Nicholas, Volume of fluid (VOF) method for the dynamics of free boundaries, J. Comp. Phys. 39 (1981) 201–225.
[2] W.J. Rider, D.B. Kothe, Reconstructing volume tracking, J. Comp. Phys. 141 (1998) 112–152.
[3] D. Gueyffier, J. Li, R. Scardovelli, S. Zaleski, Volume-of-fluid interface tracking with smoothed surface stress methods for three-dimensional flow, J. Comp. Phys. 152 (1999) 423.
[4] J.E. Pilliod, E.G. Puckett, Second-order accurate volume-of-fluid algorithms for tracking material interfaces, J. Comp. Phys. 199 (2004) 465.
[5] D.J. Benson, Computational methods in Lagrangian and Eulerian hydrocodes, Comput. Meth. Appl. Mech. Eng. 99 (1992) 235–394.
[6] D.J. Benson, Volume of fluid interface reconstruction methods for multi-material problems, Appl. Mech. Rev. 55 (2) (2002) 151.
[7] J.D. Kershner, C.L. Mader, 2DE: a two dimensional continuous Eulerian hydrodynamic code for computing multi-component reactive hydrodynamic problems, LANL (1972) LA-4846.
[8] E. Aulisa, S. Manservisi, R. Scardovelli, S. Zaleski, A geometrical area-preserving volume-of-fluid advection method, J. Comp. Phys. 192 (2003) 355.
[9] W.F. Noh, P. Woodward, SLIC (Simple Line Interface Calculation), vol. 59, Springer-Verlag, Berlin.
[10] D.L. Youngs, Time dependent multi-material flow with large fluid distortions, in: K.W. Morton, M.J. Baines (Eds.), Numerical Methods for Fluid Dynamics, Academic Press, 1982, pp. 273–285.
[11] G.R. Price, G.T. Reader, R.D. Rowe, J.D. Bugg, A piecewise parabolic interface calculation for volume tracking, in: Proceedings of Sixth Annual Conference of the Computational Fluid Dynamics Society of Canada, University of Victoria, Victoria, British Columbia, 1998.
[12] M. Rudman, Volume tracking methods for interfacial flow calculations, Int. J. Numer. Meth. Fluids 24 (1997) 671–691.
[13] D. de Niem, E. Kuhrt, U. Motschmann, A volume-of-fluid method for simulation of compressible axisymmetric multi material flow, Comput. Phys. Commun. 176 (2007) 170–190.
[14] D.J. Benson, Eulerian finite element methods for the micromechanics of the heterogeneous materials: dynamic prioritization of material interfaces, Comput. Meth. Appl. Mech. Eng. 151 (1998) 343–360.
[15] S. Mosso, S. Clancy, A geometrically derived priority system for Youngs interface reconstruction, Technical Report LA-CP-95-81, LANL, 1994.
[16] J. Osher Stanley, P. Fedkiw Ronald, Level Set Methods and Dynamic Implicit Surfaces, Springer-Verlag, 2002. ISBN 0-387-95482-1.
[17] A. Sethian James, Level Set Methods and Fast Marching Methods: Evolving Interfaces in Computational Geometry, Fluid Mechanics, Computer Vision, and Materials Science, Cambridge University Press, 1999. ISBN 0-521-64557-3.
[18] S.E. Hieber, P. Koumoutsakos, A Lagrangian particle level set method, J. Comp. Phys. 210 (2005) 342–367.
[19] Hyung Taek Ahn, Mikhail Shashkov, Mark A. Christon, The moment-of-fluid method in action, Commun. Numer. Meth. Eng. Biomedical Appl., doi:10.1002/cnm.1135.
[20] Dyadechko Vadim, Shashkov Mikhail, Reconstruction of multi-material interfaces from moment data, J. Comp. Phys. 227 (2008) 5361–5384.
[21] D.L. Youngs, An Interface Tracking Method for a 3D Eulerian Hydrodynamic code, Technical Report 44/92/35, AWRE, 1984.
[22] E.G. Puckett, A volume-of-fluid interface tracking algorithm with applications to computing shock wave refraction, in: H. Dwyer (Ed.), Proceedings of the Fourth International Symposium on Computational Fluid dynamics, Davis, CA, 1991, pp. 933–938.
[23] Keh-Ming Shyue, A wave-propagation based volume tracking method for compressible multicomponent flow in two space dimensions, J. Comp. Phys. 215 (2006) 219–244.
[24] H.R. Anbarlooei, K. Mazaheri, Moment of fluid (MOF) interface reconstruction method in multi-material arbitrary Lagrangian Eulerian (MMALE) algorithms, Comput. Meth. Appl. Mech. Eng. (2009), doi:10.1016/j.cma.2009.08.009.
[25] Benjamin Y. Choi, Markus Bussman, A piecewise linear approach to volume tracking a triple point, Int. J. Numer. Meth. Fluids 53 (2007) 1005–1018.
[26] Milan Kuchariki, R.V. Garimella, S.P. Schofield, M.J. Shashkov, A comparative study of interface reconstruction methods for multi-material ALE simulations, J. Comp. Phys. 229 (2010) 2432–2452.